Active CMOS Array for Electrochemical Sensing of Biomolecules

Peter M. Levine*, Ping Gong†, Kenneth L. Shepard*, and Rastislav Levicky‡
*Department of Electrical Engineering and †Department of Chemical Engineering, Columbia University, New York, NY 10027
‡Chemical and Biological Engineering, Polytechnic University, Brooklyn, NY 11201
E-mail: plevine@cisl.columbia.edu, shepard@ee.columbia.edu

Abstract

We describe the design of a 4×4 active sensor array for multiplexed electrochemical biomolecular detection in a 0.25-μm-CMOS process. Integrated potentiostats sense the current flowing through the on-chip Au electrodes that result from reactions occurring at the chip surface. Preliminary experimental results include cyclic voltammetry of several redox species and application to DNA probe coverage characterization.

1. Introduction

Quantitative and specific detection of biomolecules such as DNA and proteins have numerous applications in biomedical diagnostics and environmental monitoring. DNA sensing, in particular, has broad application in genotyping, gene-expression studies, mutation detection, pharmacogenomics, forensics, and related fields in which genetic content provides crucial insight into biological function or identity [1] [2].

High-throughput, multiplexed DNA analysis is usually performed in a laboratory environment using a "microarray", a passive substrate on which thousands of single-stranded DNA (ssDNA) probe molecules arranged in a regular pattern hybridize with fluorophore-labeled target molecules. Microarray scanners employing laser sources and photomultiplier tubes can measure surface-bound target densities down to 10^6 cm^{-2} [2]. Fluorescent techniques, in addition to requiring labeled targets, do not allow real-time detection of hybridization and require bulky and expensive instrumentation, defying portability for point-of-care applications.

Electrochemical-sensing approaches, which have gained interest in recent years but are not yet as well developed as fluorescent techniques [3], rely on detecting changes occurring at the interface between a metal "working" electrode (WE) functionalized with probes and an electrolyte (containing target analyte). These offer the promise of real-time, label-free sensing and portability. A feedback circuit known as a "potentiostat" is used to apply a known potential to the WE and to measure the resulting current. Specifically, if the target molecules are labeled with "redox" tags (chemical species which gain or lose electrons due to an applied potential), probe-target interactions can be detected by measuring changes in the direct (Faradaic) current flowing across the interface [4]. Alternatively, it may be possible to perform label-free sensing by measuring only changes in displacement (non-Faradaic) current at the interface due to changes in surface charge [5]. Label-free approaches eliminate numerous steps in target preparation, reducing time and cost.

Microarray applications ultimately demand parallel detection of thousands of sensing sites. For electrochemical detection, this requires active multiplexing that can only be achieved with the integration of the WEs directly onto an active substrate containing the sensor electronics. Prior work in CMOS-based electrochemical sensing arrays has focused on specific modalities of potentiostatic sensing to simplify the electronics such as redox cycling [6] and capacitance-to-frequency conversion [7]. The complexity of electrochemical analysis, however, requires general potentiostatic functionality. Previous work has also demonstrated integrated CMOS potentiostats with off-chip electrodes [8]. In this work, we design an *array* of such generalized high-performance potentiostats with integrated electrodes.

This work was supported in part by the NIH under Grant HG003089, the FCRP C2S2 Center, and an Intel Foundation Ph.D. Fellowship.

This paper is organized as follows: Section 2 provides some background on electrochemical sensing and potentiostat operation. Section 3 describes the design of the active CMOS sensor array, including chip processing and packaging issues. Section 4 includes results from electrical characterization of the array as well as electrochemical results using the CMOS sensor to measure redox species and determine DNA probe coverages on chip. Section 5 summarizes the paper and discusses future work.

2. Electrochemical Sensing

This section describes the hardware and methods used to perform electrochemical sensing.

A. Potentiostat operation

Fig. 1 displays basic potentiostat operation. In Fig. 1(a), an Au WE is placed in an electrolyte and connected to a voltage source. Without a current return path, no current flows through the metal-solution interface as detected by the ammeter. When a second interface is added in the form of a Pt "counter" electrode (CE) in Fig. 1(b), however, current can now flow steadily through the external circuit as ions in solution accept electrons from one electrode and donate electrons to the other (Faradaic process) or transiently, as ions move to the electrodes to create space-charge regions (non-Faradaic process). It is impossible, however, to distinguish activity at the WE from that at the CE as the applied potential V is dropped across both interfaces. To alleviate this issue, a non-polarizable Ag/AgCl "reference" electrode (RE) is added as shown in Fig. 1(c). The potential V is now varied until the desired voltage between WE and RE (V_{in}) is obtained. The high-impedance voltmeter between WE and RE ensures that little current flows through the RE, maintaining this interface at equilibrium. A circuit implementation of this feedback system is shown in Fig. 1(d). The op-amp on the right establishes the control loop while the integrator on the left measures the current. This circuit can be implemented in a CMOS process and forms the basis of the integrated sensor array.

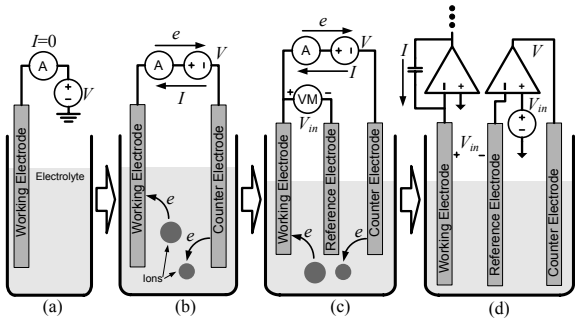

Fig. 1. Potentiostat operation and circuit implementation.

B. Sensing techniques

Different sensing modalities are determined by the nature of the applied voltage signal. "Cyclic voltammetry" (CV) is characterized by a slow voltage ramp as shown in Fig. 2(a) which causes chemical species to be oxidized or reduced at the WE when appropriate potentials are reached. Plotting the cell current versus voltage characterizes these redox potentials, and the current magnitude indicates the quantity of species that has been consumed or produced at the electrode. We use CV in Section 4 to characterize DNA probe coverages.

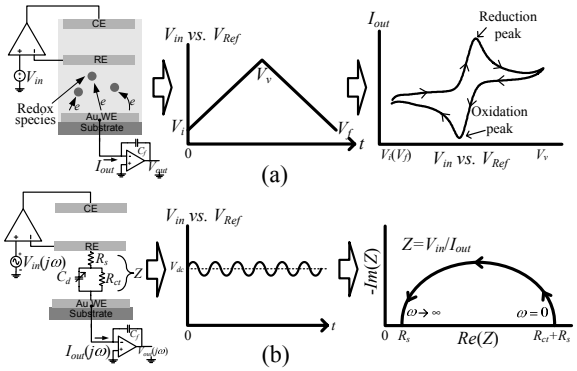

Fig. 2. Electrochemical sensing methods including (a) cyclic voltammetry and (b) impedance spectroscopy.

In "electrochemical impedance spectroscopy" (EIS), the impedance of the electrode-electrolyte interface is determined by applying a small ac voltage signal to the cell and measuring the displacement current produced as shown in Fig. 2(b). If a range of input frequencies is used, a Nyquist plot of the impedance can be made. Fitting this data to a circuit model of the interface (as shown in the figure) provides information about the "double-layer" capacitance C_d in this region. This capacitance is known to change as a function of surface charge at the WE [9].

3. Active CMOS Sensor Array Design

The overall architecture of the active CMOS potentiostat array is shown in Fig. 3 with the die photo in Fig. 4. The chip has been fabricated in a conventional 2.5-V 0.25-μm CMOS technology and measures 5 mm×3 mm. Each array site consists of a square Au WE having side lengths of 70, 80, 90, or 100 μm and a dual-slope ADC with digital control circuitry to measure the current flowing through the electrode. Each row of four electrodes shares a 15-μm×2500-μm Au CE driven by a control amplifier. The control amplifier is a two-stage, single-ended design having a simulated dc gain of 87 dB and a phase margin of 47° with an output load as large as 40 pF. This amplifier also connects to an off-chip RE.

A. ADC and supporting circuitry

Based on electrochemical measurements using a commercial potentiostat and an external Au WE having similar area as the on-chip WEs, it is determined that the on-chip ADCs must be able to digitize currents in the 100 pA–100 nA range at sampling rates up to 5 kHz. A dual-slope ADC architecture is selected to meet this goal and is shown in Fig. 5. It consists of an integrating amplifier with a fixed on-chip 5-pF linear capacitor, track-and-latch comparator, and digital counter with control logic. In the first phase, current I_{in} from the WE is integrated onto capacitor C_f for a fixed time interval t_1. In the second phase, the capacitor is discharged using the appropriate constant current source I_{ref+} or I_{ref-} until V_{int} crosses the comparator threshold at time t_2. A counter operated on ϕ_{clock} digitizes the time intervals and sets

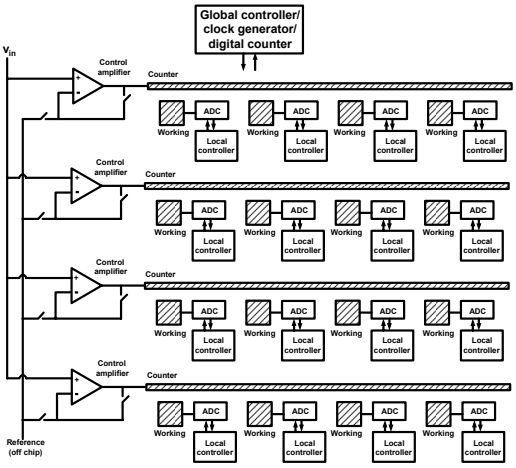

Fig. 3. Active CMOS sensor array architecture.

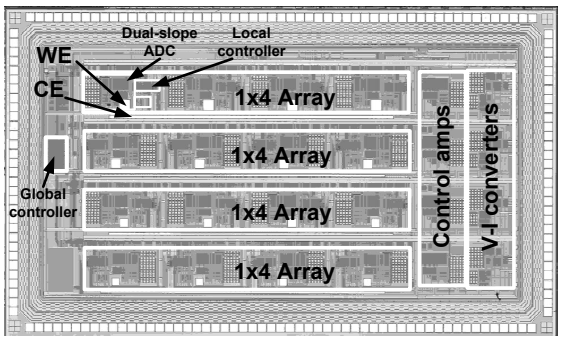

Fig. 4. Die photograph of CMOS sensor array.

the nominal resolution. Current I_{in} can then be calculated from $(t_2/t_1)I_{ref}$. Auto-zeroing for offset correction can be performed using the ϕ_{az} signal.

A conservative design approach is used in constructing the ADC components to ensure good noise performance and stability across a wide range of operating conditions. In particular, the two-stage integrator op-amp has input pFET devices of $W/L = 4.0$ mm$/1$ μm to reduce $1/f$ noise. This leads to a measured output noise voltage of 27.5 $\mu\mathrm{V_{rms}}$ over the 10 Hz–21 kHz band. To maintain closed-loop stability, the integrator op-amp is compensated with a 25-pF MIM-type capacitor and 150-Ω poly resistor between the first and second stages. This ensures an absolute minimum simulated phase margin of 45° over PVT variation and in the presence of widely-varying electrolyte impedances. The total bias current required by the integrator op-amp is a relatively large 4 mA, but heating effects have not been evident in the electrochemical measurements.

The track-and-latch comparator following the integrator is verified in simulation to operate correctly up to at least 50 MHz. Transistors M_A and M_B separate the cross-coupled switching transistors at the output from the drain of the input transistors to reduce kickback interference.

On-chip V-to-I converters have been included to test the operation of the ADCs. Each V-to-I converter contains an op-amp driving the gate of an nFET or pFET (depending on current direction) with the inverting input tied to an off-chip 10-MΩ resistor. The feedback loop ensures that the applied voltage at the non-inverting input is established across the resistor. Currents up to 150 nA can then be forced into the ADC using full-rail input voltages.

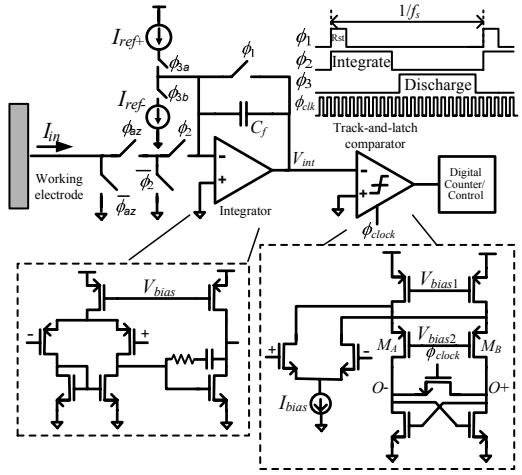

Fig. 5. Dual-slope ADC and internal circuitry at each sensing site.

B. Chip post-processing and packaging

Post-processing of the fabricated chips is necessary to create an array of Au electrodes on the surface. Au has the advantage of being relatively electrochemically inactive in the presence of strong electrolytes and is easily modified by self-assembly of well-ordered monolayers of thiols, sulfides, or disulfides through the Au-S bond [5]. As a result, thiolated ssDNA probes can be strongly bound to Au surfaces. The WEs are post-processed in a cleanroom environment by first completely etching away the top-metal Al layer and replacing it with an electron-beam-evaporated pad consisting of 20 nm of Ti (which acts as an adhesion layer) and 300 nm of Au. These directly connect to the W vias below, providing a conductive path to the active circuitry[1]. The CEs are created in a similar fashion.

The post-processed chip is set in a BGA package with the surface of the die exposed. The bond wires are shielded from electrolyte exposure through encapsulation in a heat-cured epoxy. The packaged chip is fastened in a surface-mounted PCB socket with a top-plate. A 1-mm thick polydimethylsiloxane (PDMS) sheet is added between the chip and top-plate to prevent electrolyte from leaking onto the PCB. A PVC tube is attached to the plate to form a 10-mL electrolyte reservoir above the chip.

4. Experimental Results

Measured results from electrical characterization of the dual-slope ADC and electrochemical measurements using the sensor array follow.

A. ADC characterization

DNL, INL, ac linearity, and dynamic range (DR) of the dual-slope ADC are determined using the on-chip test circuits. To allow sufficient speed to perform CV and EIS experiments, the ADC is set to a sampling rate f_s of 2.5 kHz with a ϕ_{clock} of 3.5 MHz. Integration time t_1 is set to 23 μs and discharge time t_2 is allowed a maximum of 315 μs, providing a nominal resolution of 10 bits. Additional time during each conversion cycle is required to reset the integration capacitor and select the appropriate reference current source. The maximum I_{in} before integrator saturation using these settings is about 110 nA. I_{ref+} and I_{ref-} are set to 15 nA and 18 nA, respectively. Maximum DNL and INL are measured to be -0.245 LSB and +0.376 LSB, respectively, with about a 240-pA LSB current.

DR of the ADC is verified using the on-chip V-to-I converters to deliver a sinusoidal input current at 103 Hz. Fig. 6 displays the SNDR and SNR of the ADC as a function of input current level. Averaging is used to reduce the noise current contributed by the off-chip 10-MΩ resistor. A DR of two orders of magnitude in current is visible. This is limited at the low end by the inability to provide a small enough ac voltage signal to the on-chip V-to-I converters and at the high end by integrator saturation. A maximum effective resolution (ENOB) of 9 bits is achieved and is limited by the linearity of the test circuits. Resolutions above 10 bits are achieved from simulations of the dual-slope ADC alone. Fig. 6 also shows a 4096-point FFT of the ADC output spectrum with a full-scale input.

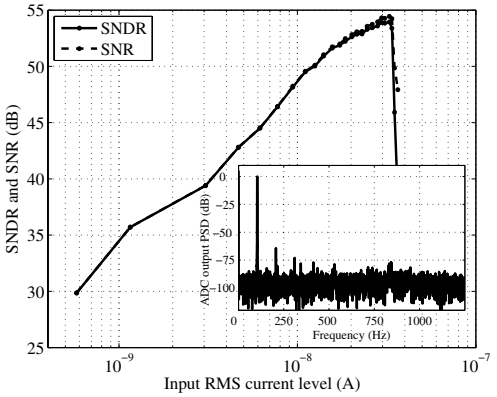

Fig. 6. Dynamic range of dual-slope ADC with characteristic output spectrum for a 103-Hz sine input (0.31 Hz Res. BW)

B. Cyclic voltammetry of potassium ferricyanide

Potassium ferricyanide $K_3[Fe(CN)_6]$ is often used by electrochemists to study interfacial properties due to its highly-reversible redox behavior. At the appropriate potential, ferricyanide ions are reduced to ferrocyanide in the reaction $Fe(CN)_6^{3-} + e \rightarrow Fe(CN)_6^{4-}$. As a first example of the use of the active CMOS sensor for electrochemical sensing, CV measurements of 2-mM potassium ferricyanide in 1-M potassium phosphate buffer (PPB, pH 7.35) are carried out. In these experiments, the potential between WEs and RE is scanned from +0.75 V to -0.5 V and back at various rates while the cell current is observed at one WE. To extend the potential range of the electrochemical cell beyond 2.5 V, an off-chip control amplifier driving a Pt-wire CE and a standard Ag/AgCl/3 M NaCl RE from Bioanalytical Systems is used. Prior to running the electrochemical experiments, the chip is first cleaned using acetone, isopropyl alcohol, and deionized water and then placed in a UV ozone cleaner for 5 min to remove organic contaminants from the surface.

The upper-left plot in Fig. 7 shows the cell current digitized at one of the 100-μm WEs with an input scan rate of 72 mV/s. A zero-phase lowpass FIR filter is used to post-process the raw data in MATLAB. The location of the forward and reverse current peaks at +0.22 V and +0.30 V, respectively, match those obtained when the same experiment is run on a CHI 700C-series commercial potentiostat using a 125-μm-diameter Au WE from ESA Biosciences.

In the bottom-right plot in Fig. 7, the CV scan rate ν is varied from 24 mV/s to 480 mV/s. It has been shown that the peak forward current i_p at a planar electrode for a reversible reaction under diffusive control is given by $i_p = kAD_O^{1/2}C_O^*\nu^{1/2}$, where

[1]We have found that this is the most effective way of preventing corrosion of the electrodes when the chip is operated in an electrolyte. When the top-layer Al is simply covered with Ti-Au, electrolyte ions pass through grain boundaries in this layer and attack the Al below.

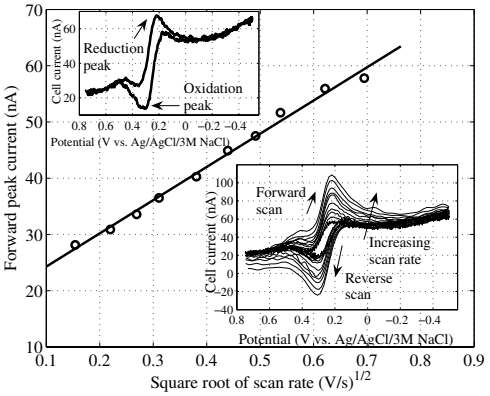

Fig. 7. Results from CV of 2-mM potassium ferricyanide in 1-M PPB captured by on-chip ADC.

k is a constant, A is the WE area, and D_O and C_O^* are the diffusion coefficient and bulk concentration of the reduced species, respectively [9]. Therefore, i_p (compared to the baseline current level) should increase linearly with $\sqrt{\nu}$ as is observed in Fig. 7.

The linear dependence of i_p on WE area is also verified by running a CV at 290 mV/s and observing the current flowing through the 100-, 90-, and 80-μm on-chip WEs. Fig. 8 shows the results from this measurement.

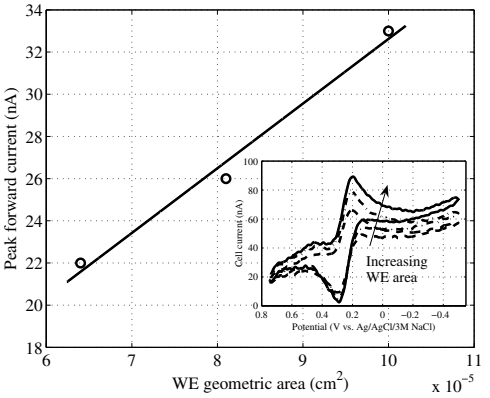

Fig. 8. Measured peak forward current dependence on WE area.

C. Determination of DNA monolayer coverages with RuHex

To demonstrate the use of the active CMOS array for biomolecular detection, the Au WEs are functionalized with a monolayer of ssDNA probes and CV is carried out using the added redox species hexaaminеruthenium(III) chloride (RuHex^{3+}) to determine changes in probe surface density. Prior work has shown that as probe coverage increases, the reduction peak potential for the reaction $\mathrm{RuHex}^{3+} + e \rightarrow \mathrm{RuHex}^{2+}$ shifts toward more negative values [10]. Such an experiment is useful in studying how the organization of nucleic acid monolayers affects probe-target binding.

The chip is cleaned as described previously and then incubated for 30 min in 0.75 μM of 20-mer DNA (sequence $\mathrm{T_7CCTTCCT_7}$–SH) in 1-M $\mathrm{MgCl_2}$ solution. Next, the chip is exposed to 1-mM mercaptopropanol solution for 90 min to passivate partially the WE surface and prevent nonspecific interactions between the immobilized DNA and WE. CV at a 4-V/s scan rate is then carried out on chip in 7 mL of 10-mM tris buffer (pH 7.4) with 1-μM RuHex.

Fig. 9 shows the results from two different CV experiments at one 90-μm WE for DNA probe coverages of 1×10^{13} cm^{-2} and 4×10^{12} cm^{-2}. These probe densities are verified using a set of calibration measurements on a commercial potentiostat with 125-μm-diameter Au WE.

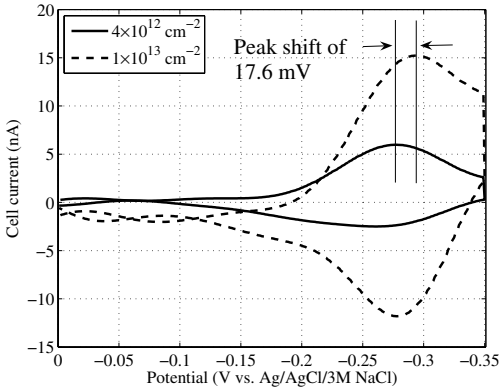

Fig. 9. CV results of DNA probe coverage determination using RuHex at on-chip WE.

The forward peaks occur at -277.2 mV and -294.8 mV for the lower and higher probe coverages, respectively. This indicates a shift of 17.6 mV toward more negative potentials with the higher coverage, confirming previous observations. Parallel experiments on a commercial potentiostat show similar peak potentials and a closely-matching shift of 15.4 mV. In addition, RuHex^{3+} concentration near the WE increases with higher probe coverages [10], explaining the observed current increase for the 1×10^{13} cm^{-2} curve. These results confirm the suitability of the active CMOS sensor array for electrochemical diagnostics.

5. Summary and Future Work

Active CMOS-integrated electrochemical sensor arrays for biomolecular detection eliminate the need for bulky and expensive optical equipment used in fluorescence-based microarrays. This paper presented the design of a 4×4 array implemented in a standard 0.25-μm-CMOS process augmented by post-processing to fabricate integrated electrochemically-compatible electrodes. Integrated potentiostat electronics and ADCs stimulate and measure electrochemical reactions occurring at the chip surface. Experimental CV results of redox behavior and measurements of DNA probe coverages were presented. Future work will involve exploiting this array for redox-labeled-target experiments and electrochemical impedance spectroscopy for label-free hybridization detection.

References

[1] M. F. Templin et al., *Trends Biotechnol.*, **20**, pp. 160–166, Apr. 2002.
[2] M. Schena et al., *Trends Biotechnol.*, **16**, pp. 301–306, July 1998.
[3] S. Szunerits et al., *Electroanalysis*, **17**, pp. 2001–2017, Nov. 2005.
[4] A. Anne et al., *J. Am. Chem. Soc.*, **128**, pp. 542–547, Dec. 2006.
[5] C. Berggren et al., *Electroanalysis*, **11**, pp. 156–160, Mar. 1999.
[6] M. Schienle et al., *J. Solid-State Circuits*, **39**, pp. 2438–2445, Dec. 2004.
[7] C. Stagni et al., *J. Solid-State Circuits*, **41**, pp. 2956–2964, Dec. 2006.
[8] R. J. Reay et al., *ISSCC Dig. Tech. Papers*, pp. 162–163, 1994.
[9] A. J. Bard et al., "Electrochemical Methods," John Wiley, 2001.
[10] G. Shen et. al, *J. Am. Chem. Soc.*, **128**, 8427–8433, June 2006.